Eur Biophys J (1999) 28: 415–426

ARTICLE

Alexander D. MacKerell Jr. · Gil U. Lee

Structure, force, and energy of a double-stranded DNA oligonucleotide under tensile loads

Received: 2 June 1998 / Revised version: 25 January 1999 / Accepted: 11 February 1999

Abstract The end-to-end stretching of a duplex DNA oligonucleotide has been studied using potential of mean force (PMF) calculations based on molecular dynamics (MD) simulations and atomic force microscopy (AFM) experiments. Near quantitative agreement between the calculations and experiments was obtained for both the extension length and forces associated with strand separation. The PMF calculations show that the oligonucleotide extends without a significant energetic barrier from a length shorter than A-DNA to a length 2.4 times the contour length of B-DNA at which the barrier to strand separation is encountered. Calculated forces associated with the barrier are 0.09±0.03 nN, based on assumptions concerning tip and thermal-activated barrier crossing contributions to the forces. Direct AFM measurements show the oligonucleotide strands separating at 2.6±0.8 contour lengths with a force of 0.13±0.05 nN. Analysis of the energies from the MD simulations during extension reveals compensation between increases in the DNA-self energy and decreases in the DNA-solvent interaction energy, allowing for the barrierless extension of DNA beyond the canonical B form. The barrier to strand separation occurs when unfavorable DNA interstrand repulsion cannot be compensated for by favorable DNA-solvent interactions. The present combination of single molecule theoretical and experimental approaches produces a comprehensive picture of the free energy surface of biological macromolecular structural transitions.

Key words Duplex DNA oligonucleotide · Molecular dynamics · Potential of mean force calculations · Atomic force microscopy

A.D. MacKerell, Jr. (✉)
Department of Pharmaceutical Sciences,
School of Pharmacy, University of Maryland,
Baltimore, MD 21201, USA
e-mail: alex@mmiris.ab.umd.edu

G.U. Lee
Chemistry Division, Code 6177, Naval Research Laboratory,
Washington, DC 20375-5342, USA

Abbreviations *DNA* Deoxyribonucleic acid · *PMF* Potential of mean force · *MD* Molecular dynamics · *AFM* Atomic force microscopy · *BP* Basepair · *ABNR* Adopted-basis Newton-Raphson · *FJC* Freely jointed chain

Introduction

Inter- and intramolecular forces can now be directly measures at a submolecular level using a variety of experimental techniques, e.g., micropipette, magnetic tweezers, optical tweezers, and atomic force microscopy (AFM). The measurement of intermolecular forces between biotin-streptavidin (Florin et al. 1994; Lee et al. 1994b; Moy et al. 1994; Chilkoti et al. 1995), DNA strands (Lee et al. 1994a; Noy et al. 1997), and several ligand-receptor systems (Evans et al. 1991; Damer et al. 1995; Hinterdorfer et al. 1996) and intramolecular forces in DNA (Smith et al. 1992; Lee et al. 1994a; Cluzel et al. 1996; Smith et al. 1996), polysaccharides (Rief et al. 1997b), and the protein titin (Kellermayer et al. 1997; Rief et al. 1997a; Tshkovrebova et al. 1997) have produced new insight into the magnitude of the forces and length scales involved in molecular recognition and the secondary structure of proteins, polynucleotides, and polysaccharides. Theoretical studies, motivated by the experimental studies cited above, have attempted to obtain atomic detail descriptions of events associated with the measured force-displacement curves (Berendsen 1996). While new insights into structure-function relationships of biological macromolecules have been obtained, both the experimental and theoretical methods applied to date have been somewhat limited. In this paper we present advances in both theoretical and experimental methodologies for the study of force-displacement behavior in biological macromolecules and show that these advances allow for a more in-depth understanding of the atomic events occurring in biological systems under tensile force.

Single molecule intramolecular force measurements via AFM have been made on polynucleotide, polypeptide,

and polysaccharide systems (Lee et al. 1994a; Rief et al. 1997a, b). In these studies polymers, often of unknown lengths, have been stretched between unknown points on the probe and the surface. Lack of knowledge of the points of contact severely limits the accessible information relating length scales to measured forces. For example, if the points of attachment on the probe and surface are significantly displaced from each other then, (1) the actual tensile force on the molecule will not be parallel with the molecular axis, leading to large uncertainties in the measured forces, and (2) the repulsive wall encountered when the tip and surface come into contact will not correspond to the true zero length of the interacting molecules, leading to errors in the measured lengths. This limitation has been overcome in the present study by using statistical centering to define the exact point-of-contact in macromolecules of defined structure, rather than the more typical "flyfishing" type experiments on homopolymers with a polydispersed molecular weight range (Rief et al. 1997b). The use of well-defined points of contract represents a breakthrough in our ability to make single molecule force measurements and relate them to molecular structure.

Theoretical studies to interpret experimental force-displacement curves have been performed using empirical force field calculations, allowing for atomic details to be obtained (Berendsen 1996; Cluzel et al. 1996; Grubmüller et al. 1996). Published studies, however, have been limited to a large extent by available computational resources. Computations on the end-to-end extension of DNA have been performed in the absence of solvent and with symmetry enforced on the molecule (Cluzel et al. 1996; Konrad and Bolonick 1996; Lebrun and Lavery 1996). While these calculations gave useful insights concerning structural changes in DNA during extension, the omission of solvent greatly limits the application of the derived models to the experimental regime. This is especially evident considering the results presented below. Molecular dynamics (MD) based studies of the streptavidin-biotin system have been performed in the presence of the solvent environment; however, pulling rates applied in those calculations exceeded the experimental values by eight orders of magnitude, requiring significant extrapolation from the theoretical regime to make direct comparison with experiment (Grubmüller et al. 1996; Evans and Ritchie 1997).

Further complications hindering a direct link between experimental and theoretical rupture forces is the realization that the experimental rupture events are not equilibrium events (Evans and Ritchie 1997). Unfortunately, the relevant nonequilibrium energies cannot measured using conventional calorimetry. Moreover, interpretation of these measurements has been limited by the fact that the intermediate molecular structures are not readily accessible via conventional techniques such as X-ray crystallography and NMR spectroscopy.

Presented here are theoretical and experimental studies on the end-to-end extension and ultimate strand separation of a DNA duplex under tensile force. Theoretical studies involve a potential of mean force (PMF) calculation based on all-atom MD simulations on the extension of a $d(ACTG)_3$ duplex. This computation was massive due to the use of explicit water and counterions, appropriate equilibration periods allowing for elimination of artifacts associated with pulling rates, and the lack of symmetry restraints. AFM experiments, based on a novel point-of-contact approach, yield force and displacement data on the end-to-end extension of DNA of greater accuracy than has been previously obtained. Near quantitative agreement is obtained between the theoretical results and experimental measurements concerning both the magnitude of the rupture force and the rupture distance. Detailed analysis of the theoretical results reveals, for the first time, the important role that solvent plays in the deformation of DNA under tensile load. These results represent a major breakthrough in the way we think about intra- and intermolecular forces, demonstrating that detailed simulations can provide valuable insight into the energetics and structure of single molecule interactions.

Following this Introduction is the Methods section that includes details of both the computational and experimental approaches. This is followed by the Results and discussion section, which have been separated into subsections presenting the theoretical data, experimental data, comparison of theoretical and experimental data, and an atomic detail interpretation of the extension of duplex DNA under tensile load. A brief summary is presented in the Conclusion.

Methods

Computational

All computations were performed on the double-stranded DNA (dsDNA) $d(ACTG)_3$-$d(CAGT)_3$ dodecamer. This sequence was selected based on its use in previously reported AFM experiments (Lee et al. 1994a). Use of a dodecamer, versus a longer oligomer, was due to computational considerations.

Calculations were performed with the program CHARMM (Brooks et al. 1983) using the CHARMM22 all-hydrogen nucleic acid parameters (MacKerell et al. 1995) in which minor modifications of the phosphodiester charges and torsional parameters had been performed (MacKerell 1997b). All MD simulations were performed in the isobaric, isothermal ensemble (Feller et al. 1995), unless noted, using the Leapfrog integrator, an integration time step of 0.002 ps and SHAKE of all covalent bonds involving hydrogens (Ryckaert et al. 1977). Atom based truncation using shift electrostatic and switch van der Waals functions with a 1.4 nm cutoff for atom-pair lists, a 1.2 nm cutoff for nonbonded interactions, and 1.0 nm distance for initiation of the vdW smoothing function was applied for all calculations, with list updates performed heuristically. Computations were initiated with the canonical A or B forms of DNA (Arnott and Hukins 1973; Arnott et al. 1973) which were overlaid with a preequilibrated solvent box of the CHARMM TIP3P water model (Jorgensen et al. 1983;

Reiher 1985) and sodium ions. All solvent molecules with a non-hydrogen atom within 0.19 nm of any DNA nonhydrogen atom were deleted and sodium ions added or deleted at random positions in the box as needed to render the system electrostatically neutral. All subsequent calculations were performed in the presence of periodic boundary conditions. The structures were then minimized for 200 adopted-basis Newton-Raphson (ABNR) steps with all DNA nonhydrogen atoms fixed and all water oxygen atoms subjected to harmonic constraints of 200 kcal/mol/nm^2. The minimized systems were then subjected to a 20 ps isothermal, constant volume MD simulation with all DNA atoms fixed. The final structures from the simulations were subjected to a 50-step ABNR energy minimization with harmonic constraints of 200 kcal/mol/nm^2 applied to all nonhydrogen atoms. The systems were then subjected to 300 ps MD simulations with harmonic distance constraints between the strand 1 and strand 2 terminal C5′ atoms using force constants of 2500 kcal/mol/nm^2 and distances of 3.0 nm and 4.5 nm, approximating the A and B forms of DNA, respectively. The final structures from these simulations were used to initiate the PMF calculations.

PMF calculations to study the end-to-end extension of DNA used a reaction coordinate defined as the terminal C5′ atom of strand 1 to terminal C5′ atom of strand 2 distance (r). Use of the C5′ to C5′ distance yields a total length of 4.5 nm, corresponding to canonical B-DNA. This value includes the 0.338 nm/bp plus 0.42 nm (0.21 nm×2) for the additional length associated with the use of the C5′ atoms at each termini. The canonical A form of DNA has a C5′ to C5′ distance of 2.7 nm, significantly shorter than the value expected for an axial rise/bp of 0.26 nm due to the 20° tilt of the basepairs. Extraction of the free energy profile was performed using the umbrella sampling method (McCammon and Karplus 1979; Northrup et al. 1982). Briefly, the reaction coordinate is systematically sampled via MD simulations (Allen and Tildesley 1989) at different r values and the energies associated with the umbrella potential required to maintain the system at that distance are calculated. This approach allows a free energy profile to be obtained for the sampled region of the reaction coordinate and has previously been successfully applied to the study of RNA di- and trinucleotides (Norberg and Nilsson 1995a, b, 1996a). In the present study we vary r for the dsDNA dodecamer from 2.0 nm, through the A (2.7 nm) and B (4.5 nm) forms of DNA, and out to 11.5 nm in 0.05 nm increments.

MD simulations for the PMF determination were performed with an initial 2 ps equilibration followed by 10 ps of sampling at a given distance. The harmonic distance constraint was then increased or decreased by 0.05 nm and the next 2 ps of equilibration and 10 ps of sampling performed. These were continued until the DNA protruded from the solvent box, at which time the calculation was halted and the system overlaid with additional waters as described below. For the PMF presented in Fig. 1A the simulations were initiated from the 3.0 nm equilibrated structure and distances sampled down to 2.0 nm and up to 4.45 nm. Sampling from 4.5 to 11.5 nm was performed from the 4.5 nm equilibrated structure. An additional 10 ps of sampling at each window was performed by restarting the initial 10 ps of sampling with the harmonic distance constraint at the same distance. Calculation of the PMF was performed using the weighted histogram procedure (Kumar et al. 1992) with the C5′ to C5′ distance stored every 0.01 ps.

At each stage of the PMF calculation when the DNA began to protrude from the solvent box, the structures were reoriented such that the strand 1 and strand 2 terminal C5′ atoms were aligned along the X axis. The systems were then overlaid with a preequilibrated box of water. The size of the waterbox was adjusted to ensure that all DNA atoms were a minimum of 0.75 nm from the edge of the waterbox in the Y and Z directions and the X direction was extended approximately 1.5 m beyond the DNA atoms. Following the overlay, all new water molecules whose oxygen atom was within 0.26 nm of any previously positioned nonhydrogen atom was deleted and the total box trimmed to the desired X, Y, and Z dimensions. In some instances this trimming deleted sodium ions; these were replaced at random positions in the system to maintain electrostatic neutrality. These systems were then minimized, subjected to a 20 ps MD simulation with the DNA fixed followed by additional minimization as described above for the initial equilibration. This was followed by an additional 20 ps isobaric, isothermal simulation in the presence of the 2500 kcal/mol/nm^2 harmonic distance constraint between the strand 1 and strand 2 terminal C5′ atoms at the distance required for that stage of the PMF calculation. The final time frame of the 20 ps simulation was used to initiate the PMF simulations. For the individual simulation systems the ionic strengths varied from 0.15 to 0.18 and DNA concentrations from 13.5 to 15.8 mM.

Experimental

The complementary oligonucleotides 5′-CAGT-CAGT-CAGT-CAGT-CAGT-3′ [abbreviated $(CAGT)_5$ and $(ACTG)_{16}$] were covalently attached to opposing surfaces as previously described (Chrisey et al. 1996; Lee et al. 1996). The AFM used in this study was designed specifically for force measurements in liquids and is based on an optical-lever displacement sensor (Meyer and Amer 1988). The instrument was operated in a variable force mode in which the surface was ramped toward the probe at velocities of 10 to 0.1 nm/s until a repulsive force of 1 nN was sensed. The displacement sensitivity of the piezoelectric transducer was determined with a capacitance sensor and fit with a second-order polynomial at various voltages. The relative surface-probe displacement was calculated by subtracting the displacement of the cantilever from the displacement of the surface. Silica spheres, 30 μm in diameter, were attached to silicon oxynitride-microfabricated cantilevers (Park Scientific Instruments, Sunnyvale, Calif.) using a chemically inert epoxy. The spring constant of each cantilever was measured at the point of probe contact with single-crystal silicon calibration standards (Tor-

tonese and Kirk 1997). Calibration with the silicon standards indicate that calibration with gold test springs (Lee et al. 1994a) overestimated the spring constants by a factor of approximately 2.

Results and discussion

In this section we present data from a combined theoretical and experimental study on the end-to-end extension of a DNA duplex. Theoretical studies were undertaken to obtain an atomic detail interpretation of the present and previously published (Lee et al. 1994a) experiments on the interstrand interactions in duplex DNA associated with its end-to-end extension under tensile load. Detailed comparison of the theoretical and experimental results showed near quantitative agreement concerning both forces and length scales. This level of agreement validates the theoretical methods used in the present study, allowing for a detailed atomic model relating structural events to energetics to be extracted from the computations. As will be shown below, solvent-DNA interactions make a central contribution to both the energetically barrierless extension of DNA and the ultimate barrier to strand separation of the DNA duplex. These results represent a major breakthrough in the way we think about intermolecular forces, demonstrating that detailed simulations can provide valuable insight into the energetics and structure of single molecule interactions.

Potential of mean force calculations

Figure 1A shows the free energy profile for the extension of the dsDNA dodecamer from 2.0 nm to 11.5 nm. The molecule is extended from 2.0 nm through the A-DNA (2.7 nm), B-DNA (4.5 nm), S-DNA (6.8 nm) forms and out to beyond a large energy barrier at 10.1 nm, to 11.5 nm. A number of small (less than 2 kT) minima and barriers are present in the free energy profile with larger minima at 2.8 nm and in the vicinity of 9.0 nm. The 2.8 nm minimum corresponds to the A form of DNA. The presence of this minimum is consistent with MD simulations using the CHARMM22 all-hydrogen nucleic acid parameter set showing the A form of DNA to be favored over the B form (Norberg and Nilsson 1996b; Yang and Pettitt 1996; MacKerell 1997a). The two minima in the vicinity of 9.0 nm are suggested to be associated with atomic rearrangements of the system prior to the barrier crossing at 10.1 nm. PMFs from the 0–10 ps and 10–20 ps sampling periods for displacements of 8–11 nm are included in the inset of Fig. 1A. The depth of the minima decreases upon going from the first to the second 10 ps of sampling, supporting the suggestion that these minima are associated with sampling limitations. The minima in the vicinity of 9.0 nm, along with the number of small minima throughout the surface, suggest that additional sampling may be required for full convergence of the PMF. The presence of a distinct barrier at 10.1 nm and

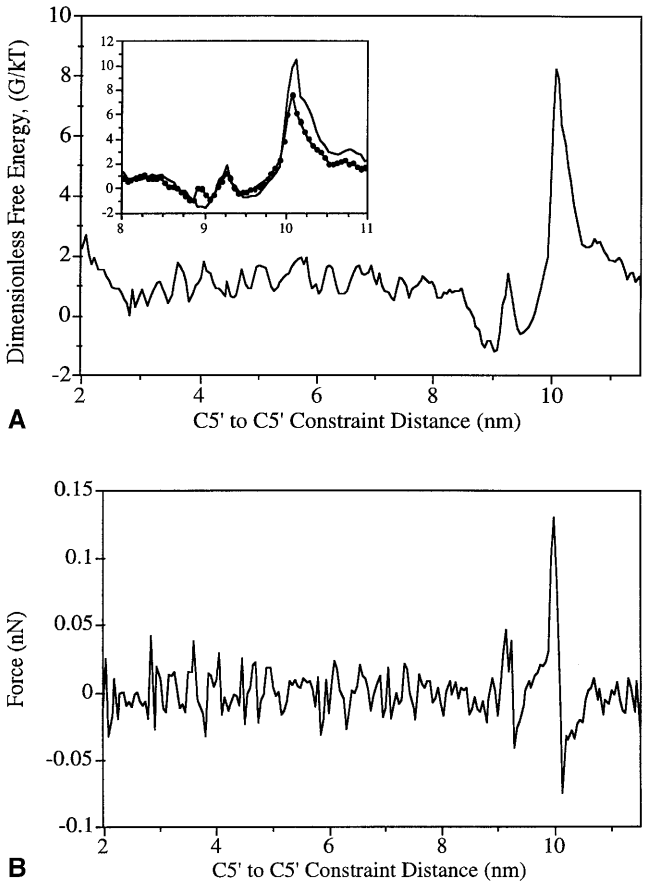

Fig. 1 **A** Calculated free energy and **B** forces for the extension of $(CAGT)_3$-$(ACTG)_3$ from 2.0 nm through 11.5 nm (kT = 0.596 kcal/mol) from the potential of mean force (PMF) calculations. Forces were determined by numerical differentiation of the free energy versus distance data in **A**. The *inset* in **A** is the PMF calculated from the 0–10 ps (*thin line*) and 10–20 ps (*thick line with dots*) sampling periods

the use of extended simulations to obtain additional energetic data at specific distances (see below, Tables 2 and 3) allow for it to be assumed that the major observations from the present calculations will not be significantly affected by additional sampling.

The most obvious feature on the surface is the barrier at 10.1 nm. This is the barrier to strand separation, occurring at 2.37 times the contour length (L_c = 2.37) of B-DNA. A barrier also occurs as the DNA is compressed towards 2.0 nm, significantly shorter than A-DNA. Compression of the DNA was performed as a test of the methodology. The expected increase in energy as the displacement approaches 2.0 nm supports the application of PMF calculations to study the extension of duplex DNA.

Previous MD simulations have shown that spontaneous conversion of A to B DNA (Cheatham and Kollman 1997) and B to A DNA (Yang and Pettitt 1996) occurs in MD simulation at room temperature. As may be seen in Fig. 1A, a number of small barriers of less than 2 kT are observed between the A and B forms of DNA at 2.8 nm and 4.5 nm, respectively. These results indicate that the barriers of 2 kT

or less between 2.8 nm and 4.5 nm in Fig. 1A are readily crossed at room temperature. Beyond 4.5 nm out to over 9.0 nm, no barriers over 2 *kT* are encountered. These results indicate that extension of DNA from 2.1 nm to greater than 9.0 nm is essentially barrierless.

AFM experiments directly measure the force-displacement behavior of a system. Accordingly, the free energy surface from the PMF was converted to a force-displacement curve and is presented in Fig. 1B. As with the PMF, the most predominate feature is observed at 10.1 nm, where a force of 0.13 nN is encountered. This force is due to separation of the strands (rupture) in the dsDNA. Calculation of the forces from the 0–10 ps and 10–20 ps sampling periods yielded 0.16 nN and 0.11 nN, respectively. Based on the difference between the 0–10 ps and 10–20 ps calculated forces divided by two, the estimated error in the calculated force is 0.025 nN. Throughout Fig. 1B a number of smaller peaks of up to 0.05 nN are present. These are attributed to noise in the calculation, although some of these events may be relevant (see below).

Atomic force microscopy experiments

A direct measurement of the force-distance behavior of the dodecamer was made with AFM using covalently end-grafted $(ACTG)_{16}$ and $(CAGT)_5$ oligonucleotides. Fig. 2A shows a single force-displacement curve measured between surfaces bearing these oligonucleotides in 0.01 M NaCl. The approach (dashed line) curve shows only repulsive forces. The repulsive wall extending to a force of 1.25 nN was used to define zero displacement. The retracting (solid line with square points) curve reveals adhesive forces which culminate in an abrupt snap away from contact at a displacement of 52.8 nm. Notable force events in the retracting curve occur at displacements of approximately 22 nm, 34 nm, and from 40 to 52.8 nm. The events at 22 nm and 34 nm correspond to adhesion forces of approximately 0.15–0.20 nN and the rupture event from 40 nm to 52.8 nm corresponds to 0.49 nN. Force events at displacements up to 22 nm can be attributed to nonspecific surface interactions. Beyond 40 nm the tensile force increases rapidly until a load of 0.49 nN is reached and the surfaces abruptly snap apart. This form of interaction cannot be attributed to Derjaguin-Landau-Verwey-Overbeek (DLVO) surface forces and is indicative of interstrand interactions (Lee et al. 1994a).

Figure 2B shows the interstrand forces from a series of AFM measurements to fall into three distinct populations centered at 0.49±0.22, 0.33±0.05, and 0.13±0.05 nN. These values are in good agreement with recent AFM experiments on a DNA 14-mer where forces of 0.46±0.18 nN were measured (Noy et al. 1997). The sequence of the oligonucleotides used in the present study makes it possible to form five complementary conformations, i.e., $(ACTG)_n$-$(CAGT)_n$ where n=5, 4, 3, 2, and 1. The stability of duplex DNA, described by the melting temperature (T_m), may be estimated using the work of Marky and Breslauer (1987). The T_m of the 12- and 8-mers in 0.01 M NaCl at an oligonucleotide concentration of 32 g/ml is 27°C and 6.2°C, respectively. Thus, only the n=5, 4, and 3 conformations are thermodynamically stable at room temperature in 0.01 M NaCl. The correlation between the number of adhesive force distributions and the thermodynamically stable interactions leads us to assign the 0.13, 0.33, and 0.49 nN adhesive force distributions to the n=3, 4, and 5 interactions, respectively.

Displacement in the AFM force-distance curve (Fig. 2A) includes contributions from the distance between and orientation of the probe-surface contact and the oligonucleotide grafting points. This displacement is related to the C5′ to C5′ constraint distance applied in the calculations (Fig. 1). The molecular grafting locations in the experiments can-

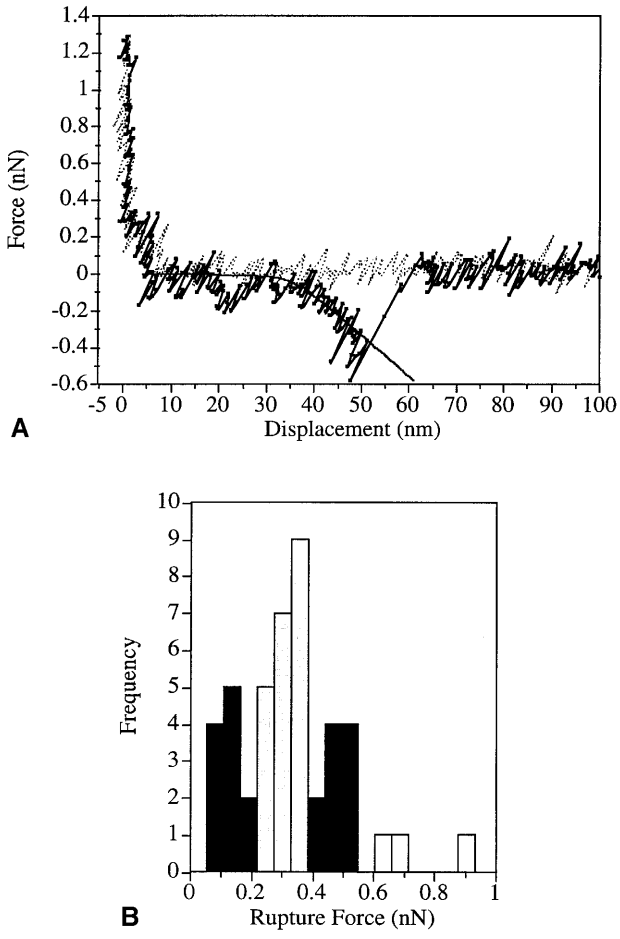

Fig. 2 **A** Force versus displacement measurement between $(ACTG)_{16}$ and $(CAGT)_5$ surfaces in 0.01 M NaCl at pH 7.0 and 25°C. *Solid line:* the elastic response described by the freely jointed chain model modified to include stretchable segments. The parameters were selected for a 64-base single-stranded DNA strand, i.e., contour length of 35.7 nm, a Kuhn segment length of 1.5 nm, and stretch modulus of 0.8 nN (Smith et al. 1992, 1996). **B** Histogram of the rupture forces resulting from 407 measurements. Rupture forces were not reported for 362 of these measurements as adhesive forces were not observed. Events associated with the n=3, 4, and 5 interactions are indicated by the different colored bars going from left to right. The three events beyond 0.6 nN (*open bars*) are due to multiple interactions (e.g. two separate duplexes forming and rupturing)

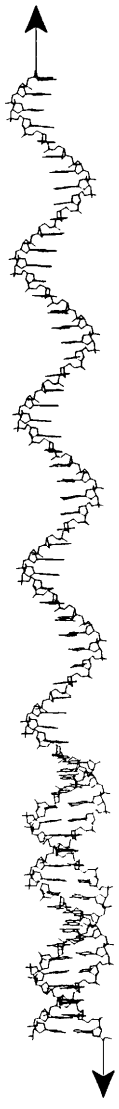

Fig. 3 Schematic diagram of the ss 64-mer interacting with the ss 20-mer assuming all basepairs in the 20-mer are involved in duplex formation and both strands are in the canonical B-form of DNA. *Arrows* represent the direction of pulling in the AFM experiment

Table 1 Experimental lengths associated with force events and theoretical lengths of the DNA total, single- and double-stranded region for a d(CATG)$_{16}$ to d(CATG)$_5$ interaction

Experimental	
Transient force event 1	22.0 nm
Transient force event 2	34.0 nm
Maximum rupture length	52.8±5.0 nm[a]
Theoretical[b]	
Canonical B for entire 64-mer	21.6 nm
Fully extended ssDNA 44-mer	35.0 nm
Canonical B dsDNA (L_c=1)	6.8 nm
Extended ss+canonical B dsDNA	41.8 nm
Extended ds DNA (L_c=2.63)[c]	17.8 nm
Extended ss+extended dsDNA	52.8 nm

[a] Error estimate based on accuracy of the data as discussed in the text
[b] Lengths calculated assuming 0.338 nm/basepair for canonical B dsDNA and 0.79 nm/basepair for fully extended ssDNA. The 0.79 nm/basepair for fully extended ssDNA was determined from a vacuum, end-to-end PMF calculation on a single-stranded dodecamer (not shown)
[c] Assuming that the accuracy of the experimental data is 5 nm (see text) yields experimental rupture distances ranging from 47.8 to 57.8 nm. These correspond to contour lengths ranging from 1.89 to 3.37, respectively. Based on this assessment, the accuracy of the experimentally determined contour length is suggested to be 2.63±0.75

not be directly controlled or determined; accordingly, the random distribution of oligonucleotides across the curved probe will produce a range of rupture lengths. The longest rupture lengths will result from interactions in which the molecular axis is aligned coaxially with the probe-surface contact. The (ACTG)$_{16}$-(CAGT)$_5$ force-distance curve presented in Fig. 2A is the longest rupture length that can be attributed to the n=5 interaction. Thus, in Fig. 2A the (ACTG)$_{16}$ 64-mer is composed of a single-stranded 44-mer and a double-stranded 20-mer. A schematic diagram of the ss and ds regions of the interacting 64-mer and 20-mer is shown in Fig. 3.

As the experimental rupture distance is obtained from one AFM run, chosen based on the point-of-contact selection criteria, there is no statistical error in the data. The accuracy of the data, however, can be estimated by the roughness of the cantilever tip and the surface and the length of the DNA to surface linkers. Both the cantilever tip and the surface have a roughness of approximately 2–10 nm (Lee et al. 1994b). The roughness will lead to the experimentally measured rupture length being 2–10 nm shorter than the actual rupture length. This is due to the zero length determined by the repulsive wall (see Fig. 2A) being associated with the highest "peak" on the surfaces while the DNA is most likely not attached to this particular peak. Opposing the surface roughness contribution is the presence of the linker between the surfaces and the DNA. The fully extended succinimidyl-4-(*p*-maleimidophenyl)butyrate linker is 2.5 nm in length as determined from modeling and minimization studies (not shown) using the ALCHEMY Program (Tripos Associates), yielding a total length of 5.0 nm for both linkers. The additional length due to the linker will make the experimentally measured rupture length longer than the actual rupture length for the DNA alone. For simplicity we assume that the contributions from surface roughness and the linker cancel and assign a value of 5.0 nm as the accuracy of the data. Supporting this assumption is the quality of fit of the modified freely jointed chain (FJC) model to the experimental data as shown in Fig. 2A. In that model the location of the curve is based on the assumed length of the DNA (Smith et al. 1996). Directly applying the assumptions used in a previous study by Smith et al. (1996) to the 64-mer used in the present study (see legend of Fig. 2), without including corrections for surface roughness or the linker lengths, yields good agreement between the modified FJC model and the experimental data.

To better interpret the force-displacement curve in Fig. 2A to structural events occurring in the DNA during

extension, some length scales based on simple assumptions must be defined. These are presented in Table 1 along with data from the experiment presented in Fig. 2 A. If the entire 64-mer is assumed to be in a canonical B form, a total length of 21.6 nm is calculated. For the single-stranded 44-mer the length at full extension is 35.0 nm. A length of 6.8 nm corresponds to the canonical B form ($L_c = 1.0$) of the ds 20-mer.

The most significant force event in Fig. 2 A is strand separation at 52.8 nm. Summation of the extented ss 44-mer length and the canonical ds 20-mer length in Table 1 yields a length of 41.8 nm. This value is what would be expected if strand separation occurred at $L_c = 1.0$, but is significantly shorter than the experimental force event at 52.8 nm. The experimental L_c at strand separation can be determined by taking the measured length of 52.8 nm, subtracting the length of the fully extended ss 44-mer, 17.8 nm, and using the difference to determine the extension per basepair for the ds 20-mer. This calculation yields a value of $L_c = 2.63 \pm 0.75$.

The other significant force events observed in Fig. 2 A and included in Table 1 are in the vicinity of 22 nm and 34 nm, associated with forces of approximately 0.15–0.20 nN. Optical tweezer (Smith et al. 1996) and micropipette (Cluzel et al. 1996) work on the end-to-end pulling of λ-phage DNA (48 kilobasepair dsDNA) show the presence of a sharp force increase of 0.05–0.08 nN as dsDNA is extended beyond $L_c = 1$, followed by additional extension to 1.7 L_c with no significant increase in force: the so-called "overstretched" transition. Comparison with calculated distances in Table 1 indicates 22 nm to be approximately equal to the length of the entire 64-mer in the canonical B form. This may be assumed to correspond to the smallest displacement at which the dsDNA will start to extend beyond the canonical B length. Previous experiments on the extension of ssDNA, however, showed significant extension beyond lengths corresponding to canonical B-DNA at forces less then 5 pN (Smith et al. 1992). Accordingly, the force event at 22 nm is assumed to be associated with nonspecific interactions and the event at 34 nm is suggested to be due to the structural transition at $L_c = 1$ seen in the optical tweezer and micropipette experiments. The magnitude of the force event at 34 nm is, however, somewhat larger than seen in the optical tweezer and micropipette experiments. The greater force and the extended displacement range over which this event occurs in the present study may be attributed to contributions from the ss region of the DNA, including intramolecular effects and intermolecular interactions with the surface or the dsDNA, or both. In better agreement with the present data is the value of 0.12 ± 0.5 nN reported for the overstretched transition in previously reported AFM experiments on the extension of duplex DNA (Noy et al. 1997).

The optical tweezer and micropipette λ-phage DNA work indicates the force distance behavior of both ds- and ssDNA to fit a modified (FJC model with similar elastic properties at $L_c > 1.6$. The modified FJC model of a 64-mer (plotted as a solid line in Fig. 2 A) fits the elastic behavior of the strand up to 48 nm displacement. The oligonucleotide behavior deviates from the FJC model beyond 48 nm. Deviation from the FJC model is attributed to a combination of strand slipping followed by strand separation. The longest measured length of a single interstrand interaction is 52.8 nm, which is 2.63 ± 0.75 L_c. This extension is significantly longer than has been measured for loads of 0.16 nN using micropipettes (Cluzel et al. 1996), although λ-phage extension lengths of 2.17 ± 0.2 L_c have been measured using capillary combine (Bensimon et al. 1995). We attribute the increased rupture length in the present experiments to slipping between the individual strands in the dsDNA that cannot occur in experimental studies using λ-phage dsDNA owing to it being composed of thousands of basepairs (see below).

Comparison of theoretical and experimental results

Single molecule data from AFM allow for direct comparison with results from MD based theoretical studies (Berendsen 1996). Use of the point-of-contact AFM approach in the present study yields excellent quality displacement data along with the sub-nN resolution force data, allowing for detailed comparison of both displacements and forces between the experimental and theoretical portions of the study.

Extraction of the distance of strand separation from the PMF in Fig. 1 A is straightforward, yielding a value of $L_c = 2.37$. For the experimental data a number of simple assumptions must be made concerning the lengths of the DNA in the ss and ds regions along with the DNA to surface linker length and surface roughness. These assumptions are discussed in the preceeding section. Based on these assumptions a contour length of 2.63 ± 0.75 is extracted from the experimental data, in good agreement with the calculated contour length of 2.37.

Recent work has emphasized that the magnitude and location of energy barriers from experimentally measured force-displacement curves may contain contributions from the tip and thermal-activated barrier crossing events (Balsera et al. 1997; Evans and Ritchie 1997; Izrailev et al. 1997). In these models the traditional transition state model is supplemented with a term to account for the mechanical energy associated with the external force, f_{ex}, acting on the system, as shown in the following equation:

$$k = \omega_0 \, e^{-(E_b - f_{ex} x)/k_B T} \quad (1)$$

where k is the barrier crossing rate, ω_0 is the vibrational frequency associated with attempts to cross the energy barrier, E_b is the intrinsic energy barrier, f_{ex} is the applied force (i.e. the force due to the cantilever tip in the present study), x is the distance over which the applied force acts prior to the barrier crossing, k_B is the Boltzmann constant, and T is the temperature. In the present study the energy barrier in Eq. (1) is associated with the free energy barrier from the PMF calculation due to both the experiments and calculations being performed in the constant temperature, constant pressure ensemble (Izrailev et al. 1997). Based on Eq. (1) it is evident that the intrinsic barrier to strand sep-

aration will be decreased by the energy associated with the tip (i.e. $f_{ex}\,x$) such that the experimentally determined barrier or force (e.g. as in Fig. 2B) is lower than the intrinsic barrier or force (e.g. that calculated via the PMF as shown in Fig. 1). This has been extended to Kramers' approach where contributions from the environment to barrier crossing, typically associated with viscous damping, are taken into account; however, the contribution from the external forces is still the same (Evans and Ritchie 1997). In the present study the reaction coordinate is described by a single reaction coordinate; however, the barrier crossing event is complicated by the large number of interactions between the two DNA strands at the barrier (see Fig. 4, 10.1 nm structure). While these interactions may be assumed to contribute to the environmental influences included in Kramers' approach, they represent a much more complex environmental contribution than, for example, viscosity effects. Indeed, barrier crossing in the present system may be considered to be more complex than the unbinding of the avidin-biotin complex, which has been discussed in detail (Balsera et al. 1997; Izrailev et al. 1997). In those studies, difficulties associated with rigorous treatment of the energy surfaces and force-displacement profiles within the context of a soft restraint (i.e. the stiffness of the spring, which may be considered a soft restraint in the present work) was emphasized. Thus, direct application of Kramers' approach in the present work may be suggested to be inappropriate, disallowing rigorous treatment of tip contributions and thermal activation to the force-displacement profile.

While rigorous treatment of tip contributions and thermal activation to the force displacement curve appears to be currently not possible, it is still desirable to estimate those contributions using simple models. First, it will be assumed that the contributions from the DNA itself (i.e. those from the PMF calculation), the cantilever tip, and thermal activation to the measured force are additive (Balsera et al. 1997). The decrease in the measured force due to tip contributions can be estimated from the spring constant of the cantilever tip, K_{tip}, used in the present study, 0.05 N/m, and the tip displacement, x. The tip displacement can be obtained from the calculated PMF in Fig. 1A, based on the distance at which the free energy initially starts to increase prior to the energy barrier to the top of the energy barrier, i.e. from approximately 9.6 to 10.1 nm. This yields a maximum tip displacement of 0.5 nm which, when multiplied by the cantilever spring constant, yields a total force contribution of 0.025 nN. Next, the decrease in the measured force due to thermal activation can be approximated by force fluctuation, δF, of the cantilever tip. These fluctuations would allow for the system to spontaneously "jump" over the barrier prior to actually reaching the top of the barrier. Estimations of the force fluctuations may be determined via $\delta F = (K_{tip}\, k_B\, T)^{1/2}$ (Balsera et al. 1997), yielding a value of 0.014 nN. Summing the tip and thermal activation contributions yields 0.039 nN as the estimate of the decrease in the calculated force from the PMF to yield the force measured experimentally. Applying this to the value of 0.13 ± 0.03 nN from the PMF yields a final computed estimate of 0.09 ± 0.03 nN. This value can be compared with experimental rupture forces of the $(CAGT)_3$-$(ACTG)_3$ dodecamer of 0.13 ± 0.05 nN in 0.01 M NaCl (Fig. 2B, $n = 3$) and 0.41 ± 0.06 nN at 0.1 M NaCl (Lee et al. 1994a). As may be seen, the computed and 0.01 M NaCl experimental values are in close to quantitative agreement. Thus, within the context of the present simplifications, satisfactory agreement between the computations and experiments occur for both the distance and force of duplex DNA strand separation. Future efforts will focus on more rigorously treating tip and thermal activation contributions to the calculated forces to allow for better comparison to experiment.

As discussed above, a significant force event in the experimental force-displacement curve occurs at approximately 34 nm (see Fig. 2A). As presented in Table 1, and consistent with previous experiments, the event at 34 nm is suggested to be associated with the extension of the dsDNA beyond the canonical B length. Such an event, however, is not seen in the calculated free energy profile nor the derived force-displacement curve shown in Fig. 1A and B, respectively. Analysis of the calculated force-displacement curve, however, shows a number of peaks in the vicinity of $L_c = 1$ (4.5 nm displacement), suggesting that the event may be within the noise of the calculated data. Possible contributions from the theoretical approaches used, including the amount of sampling and potentials used in the calculations, may also contribute (Feig and Pettitt 1997; MacKerell 1998).

Structure-energetic analysis at an atomic level of detail

To understand structural changes associated with extension and strand separation of DNA, snapshots of the structures at 2.8, 4.5, 6.75, 8.0, and 10.1 nm are presented in Fig. 4. The structures at 2.8 nm and 4.5 nm correspond to A- and B-DNA. At 6.75 nm the structure is consistent with the previously reported S form of DNA (Cluzel et al. 1996), but significant differences exist as symmetry has not been imposed on the molecule in the present calculations. Details of changes in the Watson-Crick basepairing as a function of the C5′ to C5′ constraint distance are presented in Fig. 5. The majority of basepairing is maintained through 6.8 nm. At that distance, basepair 12 opens followed by basepairs 3, 5, and 6. Basepair 1 then opens followed by simultaneous opening of basepairs 8, 9, and 10 at 7.8 nm. The remaining basepairing is maintained until opening of basepair 11 and then 2 between 9 and 9.5 nm. Only two Watson-Crick basepair interactions (basepairs 4 and 7) remain as the structure approaches the free energy barrier at 10.1 nm and both are lost as the barrier is crossed. At the barrier, two or three terminal bases are now single stranded, indicating that slipping between the strands has occurred. This slipping is not defined by frameshifting of the strands with respect to each other, as evidenced by the maintenance of basepairs 4 and 7, but rather the ability of strand-strand interactions to be lost at the termini while other Watson-Crick basepairs are still intact. In the experimental regime

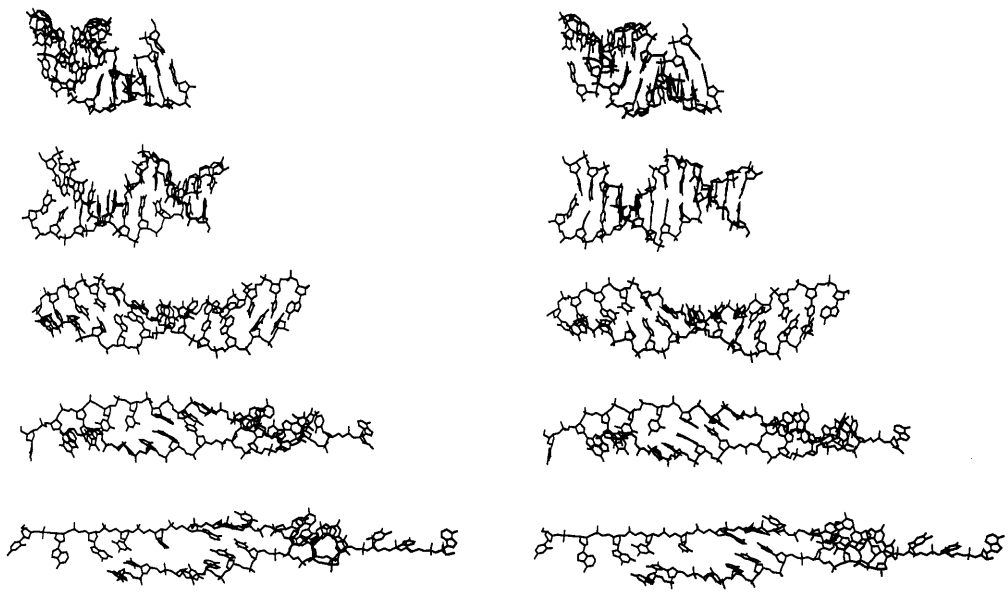

Fig. 4 Stereodiagram (crosseye) of the DNA duplex from the PMF calculations at the end-to-end distances of 2.8, 4.5, 6.75, 8.0, and 10.1 nm (*top to bottom*). Image generated using the MIDAS package (Ferrin et al. 1988)

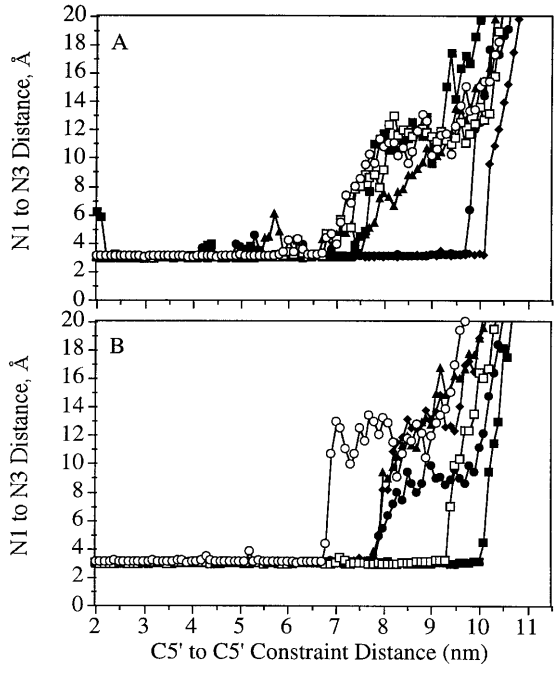

Fig. 5A, B Watson-Crick basepairing interaction distances for the individual bases versus the C5′ to C5′ displacement. **A** includes basepairs 1 through 6 and **B** basepairs 7 through 12. Watson-Crick basepairing interaction distances are based on the N1 to N3 distances and represent averages over the initial 10 ps sampling periods. Basepairs are represented as follows: 1 or 7 (■), 2 or 8 (●), 3 or 9 (▲), 4 or 10 (◆), 5 or 11 (□), and 6 or 12 (○)

it is expected that the influence of the cantilever will lead to rapid separation of the individual strands upon crossing the energy barrier, making calculated structures beyond the 10.1 nm barrier experimentally irrelevant.

To further investigate the barrierless extension of DNA and the barrier at 10.1 nm, various energetic contributions were analyzed as function of the C5′ to C5′ distance. Presented in Fig. 6 are the relative DNA-solvent interaction energies and DNA-self energy as a function of the end-to-end distance. There is a maximum in the DNA-solvent interaction energy at approximately 4.5 nm, which coincides with a minimum in the total DNA energy; this corresponds to the B form of DNA. Moving to both shorter and longer distances leads to increases in the total DNA energy and decreases in the DNA-solvent interaction energies. Extension beyond 7.5 nm leads to a rapid decrease in the DNA-solvent interaction energy. A maximum in the DNA-self energy and a minimum in the DNA-solvent interaction energy occurs at the barrier at 10.1 nm. Verification of the results in Fig. 6 was performed by continuing MD simulations at selected constraint distances for an additional 100 ps, yielding a total of 120 ps for the energetic analysis. Analysis of the resulting absolute average DNA-self and DNA-solvent interaction energies in Table 2 shows the values to be consistent with the results in Fig. 6. They suggest a model where the barrierless extension of DNA beyond 4.5 nm (Fig. 1) is due to compensation between unfavorable DNA-self energy and favorable DNA-solvent interaction energy. Similar compensatory energetics have been calculated for the unfolding of a three-helix bundle protein (Boczko and Brooks 1995).

Of note is the rapid decrease in the DNA-solvent interaction energy at 7.8 nm in Fig. 6. This decrease corresponds to the simultaneous loss of Watson-Crick hydrogen bonding of basepairs 8, 9, and 10 (see Fig. 5B). As the Watson-Crick interactions are lost, exposure of the bases to solvent increases, leading to the large decrease in the DNA-solvent interaction energy. Interestingly, this event is not associated with a significant increase in the DNA-self energy nor the free energy of the system. The lack of correlation between the loss of Watson-Crick basepairing and the free energy of the system emphasizes the role of DNA-solvent interactions as well as other DNA-self terms, in ad-

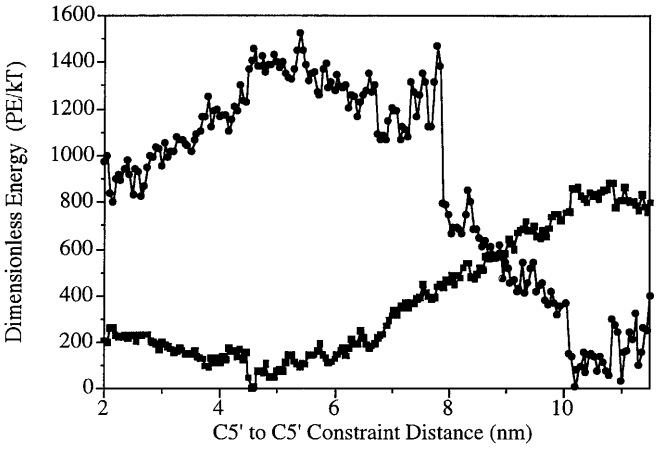

Fig. 6 Relative potential energies (kT=0.596 kcal/mol) associated with the DNA-solvent interactions (*circles*) and the DNA-self energy (*squares*) versus the C5′ to C5′ displacement. DNA-solvent represents the total interaction energy between the DNA and the solvent, including both water and salt (*circles*) and the DNA-self energy (*squares*) represents the total energy of the DNA duplex minus the DNA-solvent interaction energy. The individual energies have been offset such that the minimum energies are equal to zero. Note that the sum of the DNA-solvent and DNA-self energies does not equal the free energy due to entropic contributions

Table 3 Absolute DNA internal strand energy and the base-base, base-backbone, and backbone-backbone interstrand interaction energies from 120 ps simulations at selected constraint distances[a]

Constraint distance (nm)	Internal	Base-base	Base-bkb	Bkb-bkb
2.80	–1342±3	–260.7±0.4	–66.9±0.5	53.6±1.2
4.45	–1330±3	–252.2±0.5	–51.4±0.2	–7.4±0.2
6.75	–1305±2	–214.1±0.8	–39.9±0.6	–9.2±0.1
8.00	–1260±2	–128.5±0.5	–28.1±0.9	–2.5±0.2
9.50	–1267±1	–80.3±0.8	–12.8±0.6	47.2±0.9
10.10	–1263±4	–13.8±1.3	1.2±0.5	66.3±3.2
11.25	–1240±3	–7.5±0.2	–23.1±0.6	28.9±1.6

[a] Energies in kcal/mol. Errors represent the standard errors based on the average values from six 20 ps blocks from the 120 ps simulations. The internal energy is the total self-energy of the DNA (see Fig. 5 legend) excluding the single-strand to single-strand interaction energy. Base-base represents the interaction energy between all base atoms in strand 1 with all base atoms in strand 2. Base-backbone (bkb) is the interaction energy between all base atoms in strand 1 with all backbone atoms in strand 2 plus the interaction energy between all base atoms in strand 2 with all backbone atoms in strand 1. Bkb-bkb represents the interaction energy between all backbone atoms in strand 1 with all backbone atoms in strand 2. Backbone atoms include all atoms in the sugar and phosphodiester moieties

Table 2 Absolute DNA-solvent interaction and DNA-self energies from the 120 ps simulations at selected constraint distances[a]

Constraint distance (nm)	DNA-solvent	DNA-self energy
2.80	−5042± 8	−1616±4
4.45	−4923± 4	−1641±2
6.75	−4879± 3	−1568±2
8.00	−5245± 5	−1420±3
9.50	−5358± 7	−1313±2
10.10	−5653±18	−1210±8
11.25	−5595± 6	−1241±4

[a] Energies in kcal/mol. Errors represent the standard errors based on the average values from six 20 ps blocks from the 120 ps simulations. See Fig. 5 legend for explanation of determination of the energies

dition to Watson-Crick interactions, in stabilizing DNA structure.

It is important to reconcile previously published experiments based on optical tweezers or a micropipette (Cluzel et al. 1996; Smith et al. 1996) with the present study. Previous studies showed a sharp increase in force as the λ-phage DNA was extended past L_c=1, followed by a region where no significant increase in force was required to extend the DNA to contour lengths of 1.6–1.7. Past L_c=1.6 –1.7 a significant increase in force was required for additional extension of the molecule. As discussed above, the present calculations do not predict the event at L_c=1 seen in the λ-phage DNA; however, the results are consistent with the additional extension of the DNA followed by the significant force barrier. The ability of the λ-phage DNA to extend at constant force from L_c=1 to 1.6 may be attributed to the increase in favorable DNA-solvent interactions observed in the present calculations. At L_c=1.6, which corresponds to a C5′ to C5′ displacement of 6.95 nm, Watson-Crick basepairing is starting to be lost in the dodecamer in the present study (Fig. 5). This corresponds to extension of the DNA beyond the S form. In the dodecamer used in the present study the individual strands can "slip" with respect to each other, allowing for additional extension without encountering significant energy barriers. In the 48 kilobase λ-phage DNA it is suggested that such slipping cannot occur, leading to a significant increase in force. Thus, the barrier seen in the present study at L_c=2.4 differs from that observed in λ-phage DNA.

An understanding of the structural contributions to the energetics of the barrier at 10.1 nm may be obtained from analysis of the components of the DNA-self energy. Presented in Table 3 are the absolute energetic contributions from the DNA internal energy and strand-strand interaction energies corresponding to base-base, base-backbone, and backbone-backbone interactions for selected end-to-end distances. Interestingly, the internal energy of the DNA strands increased by less than 80 kcal/mol upon approaching the barrier while significant increases occur in the strand-strand interaction energies, accounting for the majority of the increase in the DNA-self energy in Fig. 6 and Table 2. The base-base interactions increase in a monotonic fashion, primarily due to the loss of Watson-Crick basepairing, but are still favorable at 10.1 nm. In the base-backbone interaction energies, and even more pronounced in the backbone-backbone term, is a maximum at 10.1 nm, where the interaction energies are repulsive. This maximum is associated with the backbone atoms on the individual strands coming closer together as the DNA is ex-

tended (see Fig. 4) while the DNA-solvent interaction energy continues to decrease. These results suggest the barrier to strand separation at 10.1 nm is due to the base-backbone and backbone-backbone interaction energies becoming so repulsive that the favorable DNA-solvent interactions can no longer compensate, leading to strand separation. While previous studies have shown the importance of solvent-solute interactions in structural stabilization (Boczko and Brooks 1995), the present observation represents the first atomic detail model of the contributions of solvation and structural distortions to a macromolecular barrier crossing event.

While the present computational results yield near quantitative agreement with the AFM experimental data, several limitations in the computational methodology should be reemphasized. The most obvious limitation is the initial sampling of 10 ps at each constraint distance. This has been addressed by extending the simulations at each constraint distance to 20 ps and using both the 0–10 ps and 10–20 ps data to compute the forces at the barrier (see above). However, the presence of numerous small barriers throughout PMF and the minima present in the surface at 9.0 nm and 9.5 nm indicate that additional sampling is required for total convergence of the PMF and that the presented results should be interpreted in that context. It should be noted that the conclusions associated with the DNA-self and DNA-solvent interaction energy contributions to the force-displacement profile were verified via longer simulations. Another limitation is the use of counterions at a concentration required to only neutralize the system and the change in the overall volume of the system while maintaining the same number of ions. Recent MD studies have shown that the use of only neutralizing counterions yields stable structures in the nanosecond time regime, validating the use of that approach in the present work (Norberg and Nilsson 1996b; MacKerell 1997a). Concerning the change in the total volume of the system, the ionic strength varied from a minimum of 0.15 to a maximum of 0.18 in the present study while the DNA concentration varied from 13.5 to 15.9 mM. While contributions from these changes cannot be totally discounted, it may be assumed that their influence on the present observations will be negligible. Clearly, the presented calculations do contain limiting factors; however, the level of agreement with the experimental AFM data allows for a high level of confidence that the observations made are relevant to the experimental regime. Further advances in both experimental and computational methodologies will ultimately be required to fully validate the present observations.

Conclusion

This study has shown that PMF calculations based on MD simulations can be directly linked to single-molecule force measurements made with the AFM, providing a picture of the complex structure, force, and energetics of DNA under tensile load. The narrow range of forces that are observed as DNA is extended to over twice the length of B-DNA arises from compensation of the increase in DNA-self energy by a decrease in DNA-solvent interaction energy. The effect of the extension on the dodecamer is not uniform, with different Watson-Crick basepairing interactions being lost at different displacements. A barrier to extension occurs at approximately at 2.4 L_c which is associated with interstrand repulsion that is not compensated for by favorable DNA-solvent interactions. The ability of the theoretical calculations to perform such interpretations is based on the use of detailed atomistic models, including the explicit representation of the solvent environment, yielding near quantitative agreement between calculated and experimentally determined rupture distances and forces. Further applications of combined theoretical and experimental single-molecule studies can be expected to significantly advance our understanding of the atomic contributions to the forces dictating macromolecular structure.

Acknowledgements Support is acknowledged from the DOD ASC Major Shared Resource Computing and High Performance Computing and the Naval Research Laboratory and A.D.M. acknowledges financial support from National Institute of Health Grant GM51501. Color presentations of Fig. 3 can be found at the following web page: http://www.pharmacy.ab.umd.edu/~alex.

References

Allen MP, Tildesley DJ (1989) Computer simulation of liquids. Oxford University Press, New York

Arnott S, Hukins DWL (1973) Refinement of the structure of B-DNA and implications for the analysis of X-ray diffraction data from fibers of biopolymers. J Mol Biol 81:93–105

Arnott S, Hukins DWL, Dover SD, Fuller W, Hodgson AR (1973) Structures of synthetic polynucleotides in the A-RNA and A′-RNA conformations: X-ray diffraction analyses of the molecular conformations of polyadenylic acid-polyuridic acid and polyinosinic acid-polcytidylic acid. J Mol Biol 81:102–122

Balsera M, Stepaniants S, Izrailev S, Oono Y, Schulten K (1997) Reconstructing potential energy function from simulated force-induced unbinding processes. Biophys J 73:1281–1287

Bensimon D, Simon AJ, Croquette V, Bensimon A (1995) Stretching DNA with a receding meniscus: experiments and models. Phys Rev Lett 74:4754–4757

Berendsen HJC (1996) Bio-molecular dynamics comes of age. Science 271:954–955

Boczko EM, Brooks CL III (1995) First-principles calculations of the folding free energy of a three-helix bundle protein. Science 269:393–396

Brooks BR, Bruccoleri RE, Olafson BD, States DJ, Swaminathan S, Karplus M (1983) CHARMM: a program for macromolecular energy, minimization, and dynamics calculations. J Comput Chem 4:187–217

Cheatham ITE, Kollman PA (1997) Spontaneous B-DNA to A-DNA transitions observed in the molecular dynamics simulations of d[ACCCGCGGGT]$_2$ in the presence of hexamminecobalt (III). Structure 5:1297–1311

Chilkoti A , Boland T, Ratner BD, Stayton PS (1995) The relationship between ligand-bonding thermodynamics and protein-ligand interaction forces measured by atomic force microscopy. Biophys J 69:2125–2130

Chrisey LA, Lee GU, O'Ferrall CE (1996) Covalent attachment of synthetic DNA to self-assembled monolayer films. Nucleic Acids Res 24:3031–3039

Cluzel P, Lebrun A, Heller C, Lavery R, Viovy J-L, Chatenay D, Caron F (1996) DNA: an extensible molecule. Science 271:792–794

Damer U, Popesue O, Waner P, Anselmetti P, Güntherodt H-J, Misevic GN (1995) Binding strength between cell adhesion proteoglycans measured by atomic force microscopy. Science 267: 1173–1175

Evans E, Ritchie K (1997) Dynamic strength of molecular adhesion bonds. Biophys J 72: 1541–1555

Evans E, Berk D, Leung A (1991) Detachment of agglutinin-bonded red blood cells. I. Forces to rupture molecular-point attachments. Biophys J 59: 838–848

Feig M, Pettitt BM (1997) Experiment vs force fields: DNA conformation from molecular dynamics simulations. J Phys Chem B 101: 7361–7371

Feller SE, Zhang Y, Pastor RW, Brooks RW (1995) Constant pressure molecular dynamics simulation: the Langevin piston method. J Chem Phys 103: 4613–4621

Ferrin TE, Huang CC, Jarvis LE, Langridge R (1988) The MIDAS display system. J Mol Graphics 6: 13–27

Florin EF, Moy VT, Gaub ME (1994) Adhesion forces between individual ligand-receptor pairs. Science 264: 415–417

Grubmüller H, Heymann B, Tavan P (1996) Ligand binding: molecular mechanics calculations of the streptavidin-biotin rupture force. Science 271: 997–999

Hinterdorfer P, Baumgartner W, Gruber HJ, Schilcher K, Schindler H (1996) Detection and localization of individual antibody-antigen recognition events by atomic force microscopy. Proc Natl Acad Sci USA 93: 3477–3481

Izrailev S, Stepaniants S, Balsera M, Oone Y, Schulten K (1997) Molecular dynamics study of unbinding of the avidin-biotin complex. Biophys J 72: 1568–1581

Jorgensen WL, Chandrasekhar J, Madura JD, Impey RW, Klein ML (1983) Comparison of simple potential functions for simulating liquid water. J Chem Phys 79: 926–935

Kellermayer MSZ, Smith SB, Granzier HL, Bustamante C (1997) Folding-unfolding transitions in single titin molecule characterized with laser tweezers. Science 276: 1112–1116

Konrad MW, Bolonick JI (1996) Molecular dynamics simulation of DNA stretching is consistent with the tension observed of extension and strand separation and predicts a novel ladder structure. J Am Chem Soc 118: 10989–10994

Kumar S, Bouzida D, Swendsen RH, Kollman PA, Rosenberg JM (1992) The weighted histogram analysis method for free-energy calculations on biomolecules. I. The method. J Comput Chem 13: 1011–1021

Lebrun A, Lavery R (1996) Modelling extreme stretching of DNA. Nucleic Acids Res 24: 2260–2267

Lee GU, Chrisey LA, Colton RJ (1994a) Direct measurement of the forces between complementary strands of DNA. Science 266: 771–773

Lee GU, Kidwell DA, Colton RJ (1994b) Sensing discrete streptavidin-biotin interactions with atomic force microscopy. Langmuir 10: 354–357

Lee GU, Chrisey LA, O'Ferrall CE, Pilloff DE, Turner NH, Colton RJ (1996) Chemically-Specific Probes for the Atomic Force Microscope. Isr J Chem 36: 81–87

MacKerell AD Jr (1997a) Influence of magnesium ions on duplex DNA structural, dynamic and solvation properties. J Phys Chem B 101: 646–650

MacKerell AD Jr (1997b) Influence of water and sodium on the energetics of dimethylphosphate and its implications for DNA structure. J Chim Phys Phys-Chim Biol 94: 1436–1447

MacKerell AD Jr (1998) Observations on the A versus B equilibrium in molecular dynamics simulations of duplex DNA and RNA. In: Leontis NB, SantaLucia JJ (eds) Molecular modeling of nucleic acids, vol 682. American Chemical Society, Washington, pp 304–311

MacKerell AD Jr, Wiórkiewicz-Kuczera J, Karplus M (1995) An all-atom empirical energy function for the simulation of nucleic acids. J Am Chem Soc 117: 11946–11975

Marky LA, Breslauer KJ (1987) Calculating thermodynamic data for transitions of any molecularity from equilibrium melting curves. Biopolymers 26: 1601–1620

McCammon JA, Karplus M (1979) Dynamics of activated processes in globular proteins. Proc Natl Acad Sci USA 76: 3585–3589

Meyer G, Amer NM (1988) Novel optical approach to atomic force microscopy. Appl Phys Lett 53: 1045–1047

Moy VT, Florin EF, Gaub HE (1994) Intermolecular forces and energies between ligands and receptors. Science 266: 257–259

Norberg J, Nilsson L (1995a) Stacking free energy profiles for all 16 natural ribodinucleoside monophosphates in aqueous solution. J Am Chem Soc 117: 10832–10840

Norberg J, Nilsson L (1995b) Temperature dependence of the stacking propensity of adenylyl-3′,5′-adenosine. J Phys Chem 99: 13056–13058

Norberg J, Nilsson L (1996a) Conformational free energy landscape of ApApAp from molecular dynamics simulations. J Phys Chem 100: 2550–2554

Norberg J, Nilsson L (1996b) Constant pressure molecular dynamics simulations of the dodecamer: d(GCGCGCGCGCGC)$_2$ and r(GCGCGCGCGCGC)$_2$. J Chem Phys 104: 6052–6057

Northrup SH, Pear MR, Lee CY, McCammon JA, Karplus M (1982) Dynamical theory of activated processes in globular proteins. Proc Natl Acad Sci USA 79: 4035–4039

Noy A, Vezenov DV, Kayyem JF, Meade TJ, Lieber CM (1997) Stretching and breaking duplex DNA by chemical force microscopy. Chem Biol 4: 519–527

Reiher WE III (1985) Theoretical studies of hydrogen bonding. Harvard University, Cambridge

Rief M, Gautel M, Oesterhelt F, Fernandez JM, Gaub HE (1997a) Reversible unfolding of individual titin immunoglobulin domains by AFM. Science 275: 1109–1112

Rief M, Oesterhelt F, Heymann B, Gaub HE (1997b) Single molecule force spectroscopy on polysaccharides by atomic force microscopy. Science 275: 1295–1297

Ryckaert JP, Ciccotti G, Berendsen HJC (1977) Numerical integration of the cartesian equations of motion of a system with constraints: molecular dynamics of *n*-alkanes. J Comput Phys 23: 327–341

Smith SB, Finzi L, Bustamante C (1992) Direct mechanical measurements of the elasticity of single DNA molecules by using magnetic beads. Science 258: 1122–1126

Smith SB, Cui Y, Bustamante C (1996) Overstretching B-DNA: the elastic response of individual double-stranded and single-stranded DNA molecules. Science 271: 795–799

Tortonese M, Kirk M (1997) Characterization of application specific probes for SPMs. Soc Photoptical Instrum Eng 3009: 53–60

Tskhovrebova L, Trinick J, Sleep JA, Simmons RM (1997) Elasticity and unfolding of single molecules of the giant muscle protein titin. Nature 387: 308–312

Yang L, Pettitt BM (1996) B to A transition of DNA on the nanosecond time scale. J Phys Chem 100: 2550–2566